

## Measuring spatial coupling in inhomogeneous dynamical systems

George Broze, Satish Narayanan, and Fazle Hussain

University of Houston Mechanical Engineering Department, Houston, Texas 77204-4792

(Received 15 July 1996; revised manuscript received 18 November 1996)

We propose coherence as a tool to quantify spatiotemporal dynamics, in particular, in spatially inhomogeneous dynamical systems. We demonstrate coherence to be an appropriate measure of predictability and, hence, spatial coupling in nonlinear systems, using analysis and via experimental results from a circular jet flow. Coherence measurements reveal sizable regions of strong spatial coupling in this spatially developing open flow, in contrast to much smaller coupling regions indicated by conventional correlation. Decaying coherence, indicating spatiotemporal dynamics, is also found in the jet, and possible physical mechanisms are discussed. In addition, the causes for coherence decay are explained analytically. [S1063-651X(97)00204-3]

PACS number(s): 47.20.-k, 47.27.-i

### I. INTRODUCTION

Experimental studies of spatially extended dynamical systems [1] utilize the idea of *spatial coupling*. Coupling throughout the domain indicates temporal dynamics (permitting the capture of dynamics through single-point measurements), while its spatial decay indicates spatiotemporal dynamics (requiring simultaneous measurements at multiple locations). The number and locations of probes required to describe the dynamics adequately depend on the spatial extent of coupling and the domain size, thus necessitating spatial coupling measurements. Devising an appropriate measure of spatial coupling is the goal of this paper.

Inhomogeneous systems are typified by spatially varying dynamical quantities, e.g., modal amplitude and phase. Single-mode systems can be described by a single frequency, mode shape, and phase speed or, phase envelope. In contrast, multimode systems have a spectrum of mode shapes and phase speeds, making the dynamics, particularly complex modal interactions, much more difficult to describe. In this paper, we address the spatiotemporal dynamics of inhomogeneous multimode systems. Such systems are common and of major scientific and technological interest, e.g., in open-flow hydrodynamics.

Measures often used in homogeneous spatiotemporal systems, e.g., correlation length [1,2] and dimension density [3], may be inapplicable to inhomogeneous systems due to their spatially varying length and time scales. Ordinary coherence and cross bicoherence were used to infer spatial coupling in a plane mixing layer (an inhomogeneous open flow) [4]. Spectra and bispectra (from which coherence is derived) were previously used to describe energy transfer among frequencies (accompanying transition to turbulence) in plasmas [5], in free shear layers [6] and in a Poiseuille-profile jet [7]. However, for the first time, coherence is shown here to be a reliable measure of spatial coupling.

The paper is organized as follows. In Sec II, coherence is shown to be a measure of “predictability” and of spatial coupling in dynamical systems. Coherence is compared with conventionally used correlation, and the causes of its spatial decay are analytically illustrated. A coupling measure for quadratically nonlinear systems is formulated (which can be extended to higher-order, e.g., cubic and quartic, systems). In

Sec III, experimental measurements of coherence and correlation are used to analyze spatiotemporal dynamics in an *open* flow (viz., a circular jet), and possible physical mechanisms for the observed coherence decay are analyzed. Concluding remarks are presented in Sec. IV.

### II. COUPLING IN LINEAR AND NONLINEAR SYSTEMS

By spatial coupling we mean that the dynamics at one location can be predicted using measurements at another. This implies the existence of an underlying predictive function or a dynamical system (perhaps low dimensional).

#### A. Linear model

For a linear system, the *transfer function*  $H(f)$  is used for prediction (Fig. 1). Here, we employ standard signal processing formulations with one important distinction: the input  $x(t)$  and output  $y(t)$  signals are from *spatially separated* probes. It is indeed this distinction which permits the interpretation of coherence as a measure of the spatiotemporal dynamics.

In an ideal (i.e., single-input, noise-free, linear) system with known  $H(f)$  and input, one can predict the output signal, Fourier transform, and power spectrum, respectively

$$y(t) = h(t) * x(t), \quad (1a)$$

$$Y(f) = H(f)X(f), \quad (1b)$$

and

$$G_{yy}(f) = |H(f)|^2 G_{xx}(f) \quad (1c)$$

where  $*$  denotes convolution,  $h(t)$  is the impulse response,  $H(f) = G_{xy}(f)/G_{xx}(f)$ ,  $G_{xy}$  is the cross spectrum, and  $G_{xx}$  and  $G_{yy}$  are the autospectra. Inserting  $H(f)$  into Eq. (1c) and normalizing by  $G_{yy}(f)$ , one obtains the coherence spectrum (called “coherence” or “ordinary coherence”)

$$\gamma_{xy}^2(f) \triangleq \frac{|G_{xy}(f)|^2}{G_{xx}(f)G_{yy}(f)} \equiv 1. \quad (2)$$

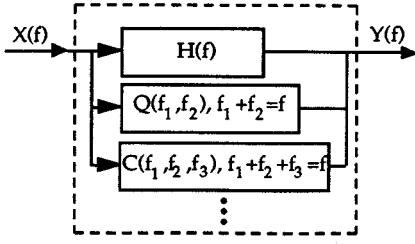


FIG. 1. Schematic of the nonlinear system model.

Given  $H(f)$ , an ideal system is completely predictable and, hence, has unity coherence.

### B. Coherence and predicted energy

In experiments, spectral quantities are estimated (denoted by “ $\hat{\cdot}$ ”) from ensemble averages. The *estimated*  $\hat{G}_{xx}$  and  $\hat{G}_{xy}$  can be used to *predict* the output spectrum (“ $\sim$ ” indicates prediction)

$$\tilde{G}_{yy} = |\hat{H}|^2 \hat{G}_{xx} = \frac{|\hat{G}_{xy}|^2}{\hat{G}_{xx}},$$

yielding the *coherence estimator*

$$\hat{\gamma}_{xy}^2 = \frac{\tilde{G}_{yy}}{\hat{G}_{yy}} = \frac{|\hat{G}_{xy}|^2}{\hat{G}_{xx} \hat{G}_{yy}}. \quad (3)$$

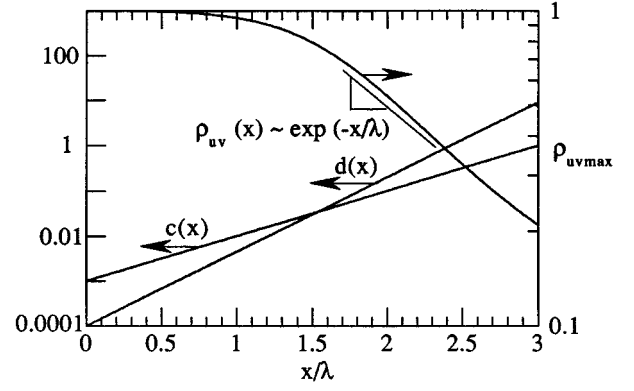
Thus, the estimated coherence is a frequency-by-frequency ratio of the predicted to the measured output energies. Moreover, since  $\tilde{G}_{yy}$  is evaluated from  $\hat{G}_{xx}$  measurements at a *different* location, coherence is a measure of *spatial coupling*. High coherence ( $\approx 1$ ) indicates strong coupling, while its difference from unity indicates the fraction of unpredictable output energy, i.e., the loss of coupling. Further, since  $|\hat{H}|^2 = \hat{\gamma}_{xy}^2 \hat{G}_{yy} / \hat{G}_{xx}$ , time series prediction also depends on coherence. Note that the estimation errors can be arbitrarily reduced given sufficiently large datasets [8] and need not contribute significantly to coherence decay. (Henceforth, we will drop the caret “ $\hat{\cdot}$ ” since all spectra discussed are estimated.)

### C. Comparison of coherence and correlation function

Correlation length  $\xi$  was used [1] to categorize dynamical systems as “large” (viz., spatiotemporal) or “small” (viz., spatially coupled) when  $\xi/\lambda \sim 1$  or  $\xi/\lambda \gg 1$ , respectively (where  $\lambda$  is some dynamically significant length scale). However, in spatially inhomogeneous systems (e.g., free shear flows), spatial growth rates and phase speeds of the various instability modes differ, making correlation inadequate for coupling measurements. Consider the simple example of a completely predictable one-dimensional spatiotemporal system with input  $u(x, t)$  and output  $v(x, t)$

$$u(0, t) = a \cos \omega_1 t + b \cos \omega_2 t,$$

$$\text{and } v(x, t) = c(x) \cos \omega_1 t + d(x) \cos \omega_2 t. \quad (4)$$

FIG. 2. Correlation decay for a fully coupled spatially developing system, with  $\xi/\lambda=1$  indicating spatiotemporal dynamics.

Since  $u$  is at the origin  $x=0$  and  $u=v$  for zero spatial separation, the coefficients  $a=c(0)$  and  $b=d(0)$ . Using any input  $u$ , and  $H(f)$  derived from Eq. (4),  $v$  can be predicted exactly. Applying Eq. (3) to Eq. (4) yields  $\gamma_{uv}^2(\omega_1) = 1$  and  $\gamma_{uv}^2(\omega_2) = 1$ , irrespective of the spatial variation of  $c$  and  $d$ . Thus, coherence is unity at the relevant frequencies and, as expected, the spatial coupling extends as far as the evolution in Eq. (4) is obeyed (i.e., to infinity, in principle). Note that even correlation will correctly indicate spatial coupling in a multimode system provided modal amplitude ratios and phase differences do not vary in space (not the general case).

Using the cross-correlation coefficient defined as  $\rho_{uv}(\tau) \triangleq [R_{uv}(\tau) / \sigma_u \sigma_v]$  (where  $R_{uv}(\tau)$  is the cross correlation,  $\sigma$  are the standard deviations, and signals  $u$  and  $v$  have zero mean), we obtain

$$\rho_{uv \max} = \frac{R_{uv}(0)}{\sigma_u \sigma_v} = \frac{(ac + bd)}{[(a^2 + b^2)(c^2 + d^2)]^{1/2}} \leq 1.$$

Thus,  $\rho_{uv \max} \equiv 1$  only if  $c/a = d/b$ , i.e., each frequency is (spatially) amplified identically. Note that, although  $G_{uv}(f) \triangleq 2 \int_{-\infty}^{\infty} R_{uv}(\tau) e^{-j2\pi f \tau} d\tau$ , (i.e., the cross correlation and the cross spectrum are a Fourier pair), additional information is obtained from  $\gamma_{uv}^2(f)$  due to its normalization by spectra (which differ at each frequency) rather than by constants as in  $\rho_{uv}(\tau)$ . A frequently used measure of spatial coupling—correlation length  $\xi$ —is based on correlation, which is expected to decay as  $\rho_{uv \max}(x) \sim e^{-x/\xi}$ ; i.e., over a distance  $x = \xi$ ,  $\rho$  decays to  $e^{-1}$  ( $\approx 37\%$ ) of its original value. At what correlation value, and, hence, what value of  $x/\xi$ , can two signals still be considered coupled? This being an unresolved issue, we will restrict our comparisons of coherence (in sec. III) to correlation only.

As a simple example, consider the amplitude evolution of  $c(x)$  and  $d(x)$  to be exponential and omit spatially dependent phases. Such exponentially growing amplitudes are commonly found in the initial (instability-dominated) regions of shear flows such as mixing layers and jets [4]. Consider coherence for spatially growing waves (Fig. 2) with  $a/b = 10$  and  $c/d = 0.5$  at  $x/\lambda = 2$ , typical of amplitude ratios (of a fundamental frequency and its subharmonic) observed in free shear flows [9]. Again, coherences at both frequencies remain unity throughout the domain, while  $\rho_{uv \max}$  rapidly

decays, with  $\xi/\lambda \approx 1$ , suggesting a limited spatial extent of coupling even when the dynamics are completely predictable.

Downstream (relative) shifts among component waves of different frequencies in dispersive systems also causes low correlation at all time delays. However, since coherence only depends on phase variations (from one realization to another) at each frequency, it can accurately detect spatial coupling in such systems.

#### D. Coherence decay

Coherence can be less than unity due to measurement noise, unmeasured uncorrelated additional inputs, or nonlinearity [8]; since measurement noise can be minimized, its effects will not be considered here. Expanding Eq. (3) in terms of ensemble-averaged Fourier spectra and substituting amplitude and phase decompositions of the form  $X_k = x_k \exp(i\phi_{x_k})$ ,  $Y_k = y_k \exp(i\phi_{y_k})$  and  $\phi_k = \phi_{y_k} - \phi_{x_k}$ , we can isolate the effects of amplitude and phase jitter on coherence. (By ‘‘jitter’’ we mean random variations of a dynamical variable.)

To study amplitude jitter, we fix the phase difference  $\phi_k$  in all realizations and obtain

$$\gamma_{xy}^2 = \frac{\langle x_k y_k \rangle^2}{\langle x_k^2 \rangle \langle y_k^2 \rangle} \leq 1, \quad (5)$$

where the ensemble averages are defined by  $\langle u_k \rangle = 1/N \sum_{k=1}^N u_k$ ,  $k$  is the realization number and  $N$  is the ensemble size. This becomes an equality if  $y_k = r x_k$  for all  $k$ ; i.e., the ratio  $r$  of the output to input amplitudes can vary with frequency but must be fixed for all realizations (in contrast to the requirement that  $r = \text{const}$  for all frequencies for  $\rho_{uv} \equiv 1$ ). As a simple example, assuming that  $y_k = r_k x_k$  and  $r_k$  is distributed uniformly on the interval  $[0,1]$ , uncorrelated with  $x_k$ , with mean  $\mu_r$  and variance  $\sigma_r^2$ , we get  $\gamma_{xy}^2 = \mu_r^2 / (\mu_r^2 + \sigma_r^2)$ , which decays with increasing  $\sigma_r^2$ .

To examine phase jitter, we hold amplitudes  $x_k$  and  $y_k$  fixed and obtain

$$\gamma_{xy}^2 = |\langle e^{i\phi_k} \rangle|^2 = |\langle \cos \phi_k + i \sin \phi_k \rangle|^2 \leq 1. \quad (6)$$

Note that it is the *difference*  $\phi_k$ , not the individual phases  $\phi_{x_k}$  or  $\phi_{y_k}$ , which affects coherence. Coherence is unity only if  $\phi_k$  is constant in all realizations. Consider  $\phi_k = \phi + s \theta_k$ , with constant  $\phi$  and a random variable  $\theta_k$  distributed uniformly on the interval  $[0, 2\pi]$ . Here,  $\gamma_{xy}^2 = \sin^2(\pi s) / (\pi s)^2$ , which decays to zero as  $s \rightarrow 1$ .

#### E. Nonlinear model

For nonlinear systems, ordinary coherence  $\gamma_{xy}^2$  may fall below unity, but this does not necessarily imply that the dynamics are less predictable. Coupling can be measured using a nonlinear system model (Fig. 1) and its coherences [5]. The procedure outlined below is applicable to systems of arbitrary order; after constructing the system model, sufficient moments and inner products can be taken to extract the transfer functions and/or coherence. However, the mathematical complexity and computational expense grow drastically with increasing order. We will restrict our discussions

to second order (i.e., to triad interactions); higher-order computations are justified only if (i) knowledge about the dynamics (e.g., the governing equations) indicates their presence (e.g., in surface gravity waves) or (ii) second-order results are substantially different from linear coherence.

The quadratic system model is

$$Y(f) = L(f)X(f) + \sum_{f_1 \geq f_2} Q(f_1, f_2)X(f_1)X(f_2), \quad f_1 + f_2 = f. \quad (7)$$

It is represented in terms of the linear and quadratic transfer functions  $L(f)$  and  $Q(f_1, f_2)$ , respectively; the first term on the right side represents linear energy transfer to the output at  $f$ , while the second term represents the cumulative contribution of all triad interactions to the output at  $f$ . Owing to symmetry with respect to  $f_1$  and  $f_2$ , the summation in Eq. (7) is restricted to  $f_1 \geq f_2$ .

Multiplying Eq. (7) by its complex conjugate, ensemble averaging and then normalizing by  $G_{yy}(f)$  yields the *total coherence*

$$\begin{aligned} \gamma_T^2(f) = & \frac{1}{G_{yy}(f)} \left[ |L(f)|^2 G_{xx}(f) \right. \\ & + \sum_{f_1 \geq f_2} |Q(f_1, f_2)|^2 D(f_1, f_2) \\ & \left. + 2 \operatorname{Re} \left\{ L(f) \sum_{f_1 \geq f_2} Q^*(f_1, f_2) A^*(f_1, f_2) \right\} \right] \leq 1, \quad (8) \end{aligned}$$

where  $A(f_1, f_2) = \langle X_k(f_1)X_k(f_2)X_k^*(f) \rangle$  (the autobispectrum) and  $D(f_1, f_2) = \langle |X_k(f_1)X_k(f_2)|^2 \rangle$ ; this assumes negligible fourth-order moments  $\langle X_k(f_1)X_k(f_2)X_k^*(f'_1)X_k^*(f'_2) \rangle$  (with  $f_1 + f_2 = f'_1 + f'_2 = f$ ), unless  $f_1 = f'_1$  [5]. Estimation errors are neglected for large ensembles.

Although each term in Eq. (8) is subject to (possibly misleading) physical interpretation, to measure spatial coupling we need only  $\gamma_T^2(f)$ . As in the linear system, total coherence indicates the predictability of output energy using measured input energy; when the input and output measurements are spatially separated, *total coherence is a measure of spatial coupling*.

Taking moments of Eq. (7) with respect to  $X^*(f)$  and  $X^*(f'_1)X^*(f'_2)$ , and ensemble averaging gives two coupled equations for  $L$  and  $Q$ , respectively [5], which can be substituted into Eq. (8) to obtain the following new *explicit* formula for total coherence

$$\gamma_T^2(f) = \gamma^2(f) \frac{|1 - \sum_{f_1 \geq f_2} \eta(f_1, f_2)|^2}{1 - \sum_{f_1 \geq f_2} \alpha^2(f_1, f_2)} + \sum_{f_1 \geq f_2} \beta^2(f_1, f_2), \quad (9)$$

where  $\gamma^2(f)$  is the ordinary coherence,  $\alpha^2(f_1, f_2) = [|A(f_1, f_2)|^2 / D(f_1, f_2)G_{xx}(f)]$  (the autobicoherence),  $\eta(f_1, f_2) = [C^*(f_1, f_2)A(f_1, f_2) / D(f_1, f_2)G_{xy}(f)]$ ,  $C(f_1, f_2) = \langle X_k(f_1)X_k(f_2)Y_k^*(f) \rangle$  (the cross bispectrum),

and  $\beta^2(f_1, f_2) = [|C(f_1, f_2)|^2 / D(f_1, f_2) G_{yy}(f)]$  is the cross bicoherence. Note that this new result does not require computationally intensive  $L$  or  $Q$  calculations to evaluate  $\gamma_T^2(f)$  [5,10]. Further, if  $A(f_1, f_2) \approx 0$ ,  $\gamma_T^2(f)$  reduces to the sum of  $\gamma^2(f)$  and  $\Sigma \beta^2(f_1, f_2)$  (simplifying computations considerably). In fact, even in the presence of substantial  $A(f_1, f_2)$ , further (heuristic) analyses suggest that a sufficient condition for high  $\gamma_T^2(f)$  is high values of both  $\gamma^2(f)$  and  $\Sigma \beta^2(f_1, f_2)$ .

For negligible autobicoherence, analytical results for total coherence decay can be obtained, analogous to the linear case: fixed amplitude ratios and phase differences give high values of total coherence, and amplitude or phase jitter cause its decay. Similar results are expected when autobicoherence is high, but analysis is difficult; some examples are examined in Appendix B.

This completes the formulation of a spatial coupling measure (viz.,  $\gamma_T^2$ ) for a quadratically nonlinear system. In contrast to prior methods, we provide an explicit and easily calculable formula for  $\gamma_T^2$ . In Sec III, experimental measurements of total coherence and correlation in an excited circular jet flow are presented.

### III. EXPERIMENTS IN A SPATIALLY DEVELOPING FLOW: THE FORCED JET

We have experimentally investigated a spatially inhomogeneous system, a free jet with a top-hat exit profile in transition from laminar to turbulent flow. The transition region is subject to several instabilities: (i) a primary Kelvin-Helmholtz instability leading to the formation of axisymmetric vortex rings (“vortex roll up”), (ii) subsequent two-dimensional subharmonic instabilities leading to the merger of neighboring vortices (vortex “pairings”), and (iii) three-dimensional instabilities leading to vortex fragmentation and transition to turbulence. The jet was acoustically excited at a single frequency  $f$ . The dimensionless control parameters are the forcing amplitude  $a_f \equiv u'_f / U_e$  and the forcing frequency  $St_D \equiv fD / U_e$ :  $u'_f$  is the centerline rms-velocity fluctuation at  $f$ ,  $U_e$  is the centerline exit velocity, and  $D$  is the jet diameter. Two periodic and two low-dimensional chaotic attractors were found over large regions in the parameter space. The experimental facility and procedures, the phase diagram, the attractors’ invariants and transitions between dynamical states are extensively discussed in [11,12].

*Spectral dynamics.* Of particular importance (to technological processes such as mixing and aerodynamic noise generation) are the formation and pairings of vortices. While the fundamental frequency  $f$  (associated with vortex roll up) is externally forced, the vortical interactions (and, hence, the associated subharmonic and quarterharmonic frequencies  $f/2$  and  $f/4$ ) are driven by feedback from vortex pairings [13], i.e., are self-excited. The spatially growing waves associated with these frequencies have linear regions in which they grow exponentially at different rates (evolving at different phase speeds), followed by nonlinear regions where they saturate at different amplitudes and grow or decay due to self-interactions and cross-interactions. The saturation of the fundamental is physically realized by vortex roll up; pairings result from the (nonlinear) subharmonic resonance phenomenon, where a fundamental and its subharmonic interact to reinforce the subharmonic (i.e.,  $f + (-f/2) = f/2$ ) [9]. Thus,

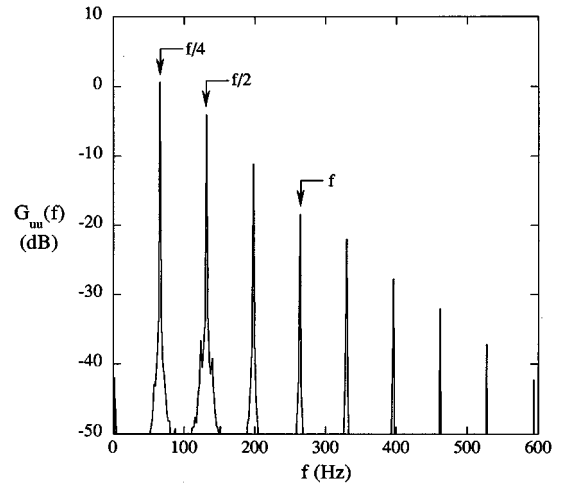


FIG. 3. Power spectrum for a periodic state, stable double pairing (SDP), with acoustic forcing at  $f$  only, displaying dynamically significant spectral peaks at the fundamental  $f$ , the subharmonic  $f/2$  and the quarterharmonic  $f/4$ , recorded at  $x/D \approx 1.75$ .

the relevant and dominant frequencies are the fundamental, the subharmonics, and the sidebands generated by detuned feedback (i.e., when feedback is not exactly at  $f/2$  and  $f/4$ ) [12]. Although the dynamics of this physical system can be relatively simple (nominally two-dimensional and limited to as few as three, or even two, instability modes), this prototypical flow embodies several important and common features of spatiotemporal dynamical systems: spatially evolving, inhomogeneous, and dispersive, with linear and nonlinear instabilities. In the following we briefly describe the salient features of a periodic and a chaotic state chosen for the present study.

The periodic state, stable double pairing (SDP), was found for  $0.01 \leq a_f \leq 0.20$  and  $1.05 \leq St_D \leq 1.60$ . Spectral peaks at  $f$ ,  $f/2$ , and  $f/4$  (see Fig. 3, recorded downstream of the first pairing location, at  $x/D \approx 1.75$ ) are due to periodic vortex roll up followed by a periodic first pairing and then a periodic second pairing of vortices downstream. For SDP, the first and second pairings occur approximately at  $x/D \approx 1.5$  and at  $x/D \approx 2.5$ , respectively [11,12]. Since the sources of  $f/2$  and  $f/4$  at the jet exit are presumably feedback from pairings, it is reasonable to expect that spatial coupling will extend at least as far as the pairing locations (and perhaps beyond, unless there are significant effects from new instabilities whose origins were not measured; see Sec. III C.

A chaotic state (the “quarterharmonic chaotic attractor,” QCA) is found in the range  $0.008 \leq a_f \leq 0.02$  and  $1.1 \leq St_D \leq 1.25$ . The power spectrum (Fig. 4) recorded near the first vortex pairing location ( $x/D \approx 2$ ) shows peaks at  $f$  and two sidebands around the subharmonic ( $f_l = f/2 - \Delta f$ ,  $f_h = f/2 + \Delta f$ ), indicating (almost) periodic subharmonic modulations, i.e., a first pairing whose location changes (nearly) periodically in space [12]. The broadband centered at  $f/4$  is due to chaotic second pairing occurring farther downstream. The waves corresponding to the modulated subharmonic and the broadband quarterharmonic have longer (than in SDP) spatial evolution times and are results of detuned pairing feedback [12]. Correspondingly, the first pairing location for QCA is delayed to  $x/D \approx 2$ , and the sec-

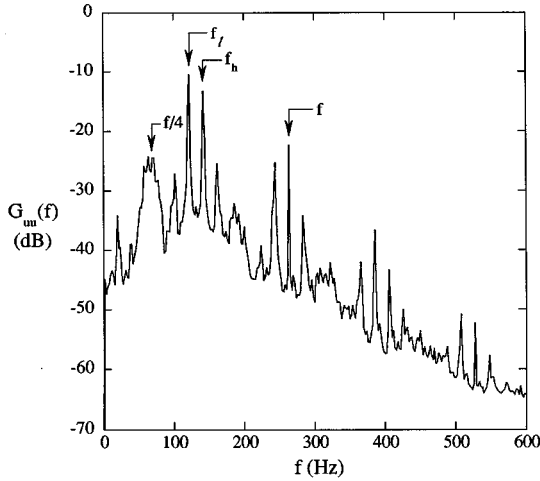


FIG. 4. Power spectrum for a chaotic state, quarterharmonic chaotic attractor (QCA), with acoustic forcing at  $f$  only, showing dynamically significant spectral peaks at the fundamental  $f$ , the lower and higher sidebands around the subharmonic ( $f_l, f_h$ ) and the center frequency of the broadband quarterharmonic  $f/4$ , recorded at  $x/D \approx 2$ .

ond pairing may occur as far as  $x/D \approx 4$ .

Below we present cross correlation and total coherence for SDP (at  $a_f \approx 2.4\%$ ,  $St_D \approx 1.2$ ) and QCA (at  $a_f \approx 1.4\%$ ,  $St_D \approx 1.2$ ), measured using hot-wire velocity probes; data acquisition was performed using a 12-bit analog-to-digital converter on a Masscomp MC6650 computer. The reference probe was positioned near the jet exit ( $x/D \approx 0$ ) and displaced radially by  $0.2D$ , with long prongs to keep the probe body out of the jet core (thus minimizing probe interference and wakes); a second probe (aligned with the jet centerline) was traversed downstream at intervals of  $\Delta x/D \approx 0.25$ .

### A. Cross correlation

The peak cross-correlation coefficient  $\rho_{x_1 x_2 \max}$  for both attractors decay rapidly (Figs. 5 and 6), falling below 0.5 by  $x/D \approx 1$ . This decay is primarily due to rapid spatial variation of the ratio of the fundamental and the subharmonic amplitudes (see Sec. II and the amplitude plots in [11]). Cor-

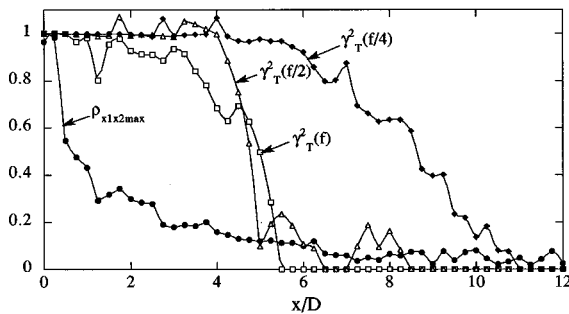


FIG. 5. Spatial variation of total coherence  $\gamma_T^2(f)$  and the peak correlation coefficient  $\rho_{x_1 x_2 \max}$  for SDP; high  $\gamma_T^2(f)$  at all frequencies indicates strong coupling at least up to  $x/D \approx 4$ , while low values of  $\rho_{x_1 x_2 \max}$  (by  $x/D \approx 1$ ) spuriously indicates the loss of coupling.

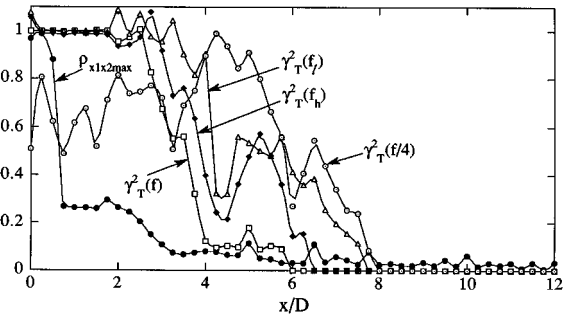


FIG. 6. Spatial variation of total coherence  $\gamma_T^2(f)$  and the peak correlation coefficient  $\rho_{x_1 x_2 \max}$  for QCA; nominally high  $\gamma_T^2(f)$  at all frequencies indicates strong coupling at least up to  $x/D \approx 4$ , while  $\rho_{x_1 x_2 \max}$  drops to very low values by  $x/D \approx 1$ .

relation diminishes well before the minimum expected coupling distance of  $x/D \approx 2.5$  (i.e., the second pairing location).

### B. Total coherence

To analyze total coherence  $\gamma_T^2$  [evaluated using Eq (9)] for the dynamically significant frequencies noted in the power spectra of SDP and QCA, 400 records of 1024 samples were averaged with a frequency resolution of 2 Hz (see Appendix A for further details).

*SDP.* Total coherences at  $f$ ,  $f/2$  and  $f/4$  remain high ( $\geq 0.8$ ) as far as  $x/D \approx 4$ , 5 and 7, respectively, (Fig. 5), indicating *spatial coupling* well beyond the second pairing location. As previously noted, this is not surprising provided new unmeasured events do not occur, i.e., events whose origins are underresolved or undetected at the first location (e.g., three-dimensional secondary instabilities). Although theoretically bound by unity,  $\gamma_T^2(f/2)$  and  $\gamma_T^2(f/4)$  slightly exceed unity at a few locations (e.g., at  $x/D = 4$ ), apparently because of insufficient spectral averaging (see Appendix A). From cross bispectra (not shown), the most significant quadratic interactions for SDP were found to be those between the fundamental and the subharmonic (i.e.,  $f + (-f/2) = f/2$ ) and those between the subharmonic and the quarterharmonic (i.e.,  $f/2 + (-f/4) = f/4$ ), culminating in the first and second vortex pairings, respectively [9].

*QCA.* Total coherences at  $f$ , the lower sideband  $f_l$  and the higher sideband  $f_h$  frequencies (shown in Fig. 6) remain above 0.8 as far as  $3 \leq x/D \leq 5$ , the region where chaotic second pairing is usually completed [12]. Again, there are slight excursions above unity in the values of  $\gamma_T^2(f_l)$  and  $\gamma_T^2(f_h)$ . The dynamically significant quadratic interactions seen (in the bispectra, not shown here) are those of (i)  $f$  and  $f_h$  (i.e.,  $f - f_h = f_l$ ), (ii)  $f$  and  $f_l$  (i.e.,  $f - f_l = f_h$ ), and (iii)  $f_l$  and  $f_h$  with frequencies in the broadband surrounding  $f/4$  (e.g.,  $f_l - f/4 = f/4 - \Delta f$  or  $f_h - f/4 = f/4 + \Delta f$ ); owing to the broadband surrounding  $f/4$ , a coarser frequency resolution of 9 Hz was chosen around that frequency for computations. High  $\gamma_T^2$  at all significant frequencies up to  $x/D \approx 4$  indicate strong spatial coupling, even in the presence of chaotic dynamics.

High values of  $\gamma_T^2$  over a large region for both periodic and chaotic vortex dynamics indicate that the transitional jet displays temporal, rather than spatiotemporal, dynamics. Cross-correlation results spuriously imply a much smaller

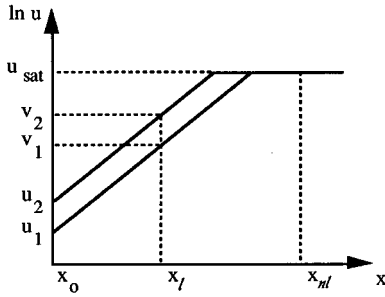


FIG. 7. Spatial development of an instability amplitude for a pair of realizations, illustrating an amplitude jitter mechanism in free shear flows.

coupled domain (i.e.,  $x/D < 1$ ) as a result of spatial inhomogeneities. Similar results were found in an excited mixing layer as well [4]. The rapid drop of  $\gamma_T^2$  downstream ( $x/D > 7$  for SDP and  $x/D > 5$  for QCA) is evidence of spatiotemporal dynamics; possible mechanisms for such disorder are discussed next.

### C. Physical mechanisms of coherence decay

As addressed in Sec. II coherence decay (indicative of coupling loss) can result from amplitude and/or phase jitter. However, the physical mechanism for such jitter may differ among dynamical systems. In the following, some such mechanisms are discussed in the context of jet flows; similar arguments may apply to other open free shear flows as well, such as wakes and mixing layers.

*Amplitude jitter.* An example of how amplitude jitter may occur in a jet is illustrated in Fig. 7, where the spatial development of the amplitude of an instability mode (viz., Kelvin-Helmholtz) is sketched for two realizations from an ensemble of different initial amplitudes; the saturation amplitudes of these modes are known to be relatively insensitive to the initial amplitudes [9]. The input amplitude  $u_k$  at  $f$  is measured at the origin  $x_0$ . In the first case, the output fundamental spectral amplitude  $v_k$  is measured at  $x_l$  in the linear range; hence, the ordinary coherence,  $\gamma_{uv}^2 = 1$  (assuming constant phase shift at  $f$  between  $x_0$  and  $x_l$ ) since the amplitude ratio  $v_k/u_k$  is constant in each realization [see Eq. (5)]. In the second case, the output spectrum is measured at  $x_{nl}$  in the nonlinear range, where  $u$  has reached its saturated value  $u_{sat}$ . Here, the amplitude ratio  $u_{sat}/u_k$  varies from one realization to another, and  $\gamma_{uv}^2 < 1$ . Similar effects may occur for the subharmonic and the quarterharmonic as well.

*Phase jitter.* Coherence can be affected by variations of the phase difference (of individual frequency components) in several ways; here, two such effects are illustrated by examining the spatial development of a resonant subharmonic wave (Fig. 8) in a jet flow. When the fundamental wave (not shown) reaches a critical amplitude at  $x_0$ , it resonates nonlinearly with and reinforces the subharmonic, thus modifying the subharmonic spatial growth rate (depending on  $\theta$ , the phase difference between the two waves) [9]. First, consider the coherence at  $f/2$  between the signals at  $x_0$  and  $x_1$ : phase jitter will be absent if the subharmonic phase speed is independent of  $\theta$ . Nevertheless,  $\theta$  variations (due to detuned feedback) result in amplitude jitter at  $x_1$  and, hence, coherence decay. In contrast, there is no amplitude jitter between

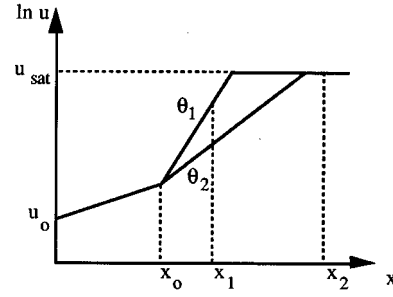


FIG. 8. Spatial development of the amplitude of a resonant subharmonic wave for different phases  $\theta_i$ , illustrating mechanisms for amplitude and phase jitter in free shear flows.

$x_0$  and  $x_2$ , but the phase after saturation (i.e., at  $x_2$ ) may not be linearly related to the phase prior to the onset of resonance (i.e., at  $x_0$ ). This phase jitter will also result in coherence loss.

Phase jitter may also be caused by the development of three dimensionality. The three-dimensional effect sketched in Fig. 9 (showing two realizations of advecting rectilinear vortices) is analogous to azimuthal instabilities of ring vortices, but is more easily understood in a planar configuration. In both realizations, the trailing vortex is rectilinear (or nearly so), but a spanwise instability (of fixed wave number but arbitrary phase) has grown on the leading vortex as it moved downstream. Coherence at the vortex passage frequency will fall below unity since the phase shift  $\phi_k$  between  $u(t)$  and  $v(t)$  varies from one realization to the next. Note that, in this case, the phase jitter is due to an unknown input (viz., the disturbances which trigger the three dimensionality). If the spanwise disturbance is present on the upstream vortex, even at low amplitudes, additional spanwise-separated probes at the upstream location might provide sufficient information to make the downstream distortion predictable (using multiple and partial coherences [8]).

### IV. CONCLUDING REMARKS

Total coherence  $\gamma_T^2(f)$  accurately identifies coupling in spatiotemporal dynamical systems, particularly inhomogeneous ones. Coherence is applicable to homogeneous systems as well; when dynamics are dominated by a single fre-

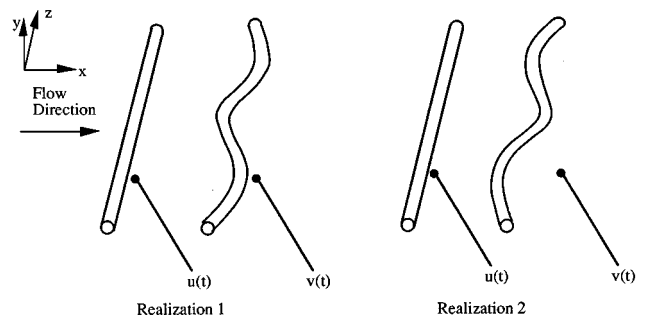


FIG. 9. Illustration of phase jitter due to random three-dimensional disturbances on rectilinear vortices in a plane free shear flow; the downstream phase at the vortex passage frequency [in  $v(t)$ ] is different in the two realizations.

quency, coherence and correlation results are identical; with multiple modes, coherence can identify frequencies and interactions responsible for coupling decay. Since coherence can be interpreted as the predictable energy fraction, this appears to be the first method for measuring predictability in multimode spatiotemporal systems. Consequently, this result is an important step in addressing the challenging problem of modeling and controlling technologically relevant spatiotemporal (*open*) flows.

To demonstrate the practical feasibility of coherence, as a spatial coupling measure, we measured total coherence in a circular jet. The results indicate large spatially coupled regions (extending from 4 to 7 jet diameters), implying high predictability of dynamics (using single-point measurements) in these flow regions. We have demonstrated that misleading estimates of spatial coupling can be inferred from correlation-based measures.

Diminished coherence comes from additional unmeasured inputs (or interactions), higher-order nonlinearity or measurement noise; these manifest themselves as jitter in amplitudes and phases of the measured dynamical variable. Mechanisms for such jitter depend on the physical system under consideration, e.g., the onset of secondary instabilities in Rayleigh-Bénard convection [14], transverse instabilities in film flows [15], three dimensionality in open shear flows [16], higher-order nonlinearities, or transition to turbulence. In the first three cases, the apparent loss of predictability can, in principle, be recovered by judicious placement of additional sensors; increasing the order of the system model will capture higher-order nonlinearities. In deterministic systems, the only “true” sources of unpredictability (given an adequate system model) are unmeasured or underresolved inputs, specifically, small fluctuations (e.g., changes in initial conditions) amplified by instabilities and/or temporal or spatiotemporal chaos.

#### ACKNOWLEDGMENTS

This work was supported by Texas ARP Grant No. 003652-151, AFOSR Grant No. F49620-92-J-0200, and ONR Grant No. N00014-94-1-0510.

#### APPENDIX A: COHERENCE COMPUTATIONS

The  $\gamma_T^2(f)$  estimation using Eq. (9) is made quite difficult by two problems: noise and spectral leakage. The summations in Eq. (9) contain many terms (up to 512 here), depending on the frequency resolution. Noise and random estimation errors at all frequencies cause residual values whose accumulation yield poor estimates of  $\gamma_T^2(f)$ . Since the random error for spectral estimation scales as  $N^{-1/2}$  (where  $N$  is the ensemble size), the cumulative error can be significant even when  $N$  is large (e.g.,  $10^2$ – $10^4$ ); to minimize these errors, we used a threshold of  $(2/N)^{1/2}$  on all spectra and bispectra. Data windowing causes leakage of coherent energy into frequencies neighboring significant coherence or bicoherence peaks, causing summations including these frequencies to be erroneously high. After testing different windows, we found rectangular windows to have minimal coherent sideband leakage [17].

Autobicoherence was computed using 200 realizations of

a synthetic signal with significant energy at a single triad,  $f_1 + f_2 = f$ , and low-amplitude random noise. The autobicoherence sum  $S = \sum_{f_1 \geq f_2} \alpha^2(f_1, f_2)$  is ideally equal to unity. This sum was evaluated after applying rectangular ( $R$ ) and Hamming ( $H$ ) windows, yielding  $S_H = 4.21$  and  $S_R = 2.04$  [with  $\alpha^2(f_1, f_2)_H \approx 1$  at two frequencies around the true peak]. After applying thresholds,  $S_H = 3.00$  and  $S_R = 1.00$ . Although the noise contribution is reduced,  $S_H$  is clearly still in error (due to spectral leakage).

In processing the experimental data, it was found that using a relatively small number of realizations (e.g., 100 records) for spectral averaging resulted in  $\gamma_T^2(f)$  exceeding 1 (its theoretical upper bound). In fact, even after the number of realizations was increased to 400, such excursions were not completely eliminated (evident in Figs. 6 and 7). We believe that these errors are attributable to noise. In practice, it may not always be possible to select a threshold which eliminates all noise while preserving all signal contributions. In general, increasing the number of realizations should diminish these excursions. For SDP at  $x/D \cong 3.75$ , calculations yielded  $\gamma_T^2(f/2) \approx 1.14$  using 100 realizations, but  $\gamma_T^2(f/2) \approx 1.07$  using 400 realizations. Also for SDP, at  $x/D \cong 3.25$ ,  $\gamma_T^2(f/4) \approx 1.14$  using 100 realizations, but  $\gamma_T^2(f/4) \approx 0.992$  using 400 realizations.

#### APPENDIX B: ANALYSIS OF TOTAL COHERENCE WITH HIGH AUTOBICOHERENCE

As noted in Sec. II E, the causes of coherence decay are difficult to interpret when autobicoherence is high. To investigate this, we used synthetic input and output signals (e.g., from spatially separated probes) of the following form.

$$\begin{aligned} u(t)|_{x=x_1} &= a_k \cos(\omega_1 + \phi_{ak}) + b_k \cos(\omega_2 t + \phi_{bk}) \\ &\quad + c_k \cos(\omega t + \phi_{ck}) + d_k \cos(\omega t + \phi_{dk}) + n_u(t) \\ v(t)|_{x=x_2} &= e_k \cos(\omega t + \phi_{ek}) + f_k \cos(\omega t + \phi_{fk}) + n_v(t), \end{aligned}$$

where  $\omega = 2\pi f$ , and  $n_u(t)$  and  $n_v(t)$  are low-amplitude band-limited white noise (at least 50 dB below  $\omega_1$ ,  $\omega_2$ , and  $\omega$  peaks). For simplicity, the two signals are provided significant energy only at three frequencies.

The key effects we expect to capture in these signals are (i) linear energy transfer at  $\omega$  between the  $d_k$  and  $f_k$  terms, (ii) autobicoherence at  $\omega_1 + \omega_2 = \omega$  using the  $a_k$ ,  $b_k$  and  $c_k$  terms, and (iii) quadratic energy transfer to  $\omega$  using the  $a_k$ ,  $b_k$  and  $e_k$  terms. To ensure high autobicoherence, the amplitude ratio  $a_k b_k / c_k$  and the phase difference  $\phi_{ck} - \phi_{ak} - \phi_{bk}$  are kept constant;  $\alpha^2(f_1, f_2) \approx 0.99$  for all cases. Pseudorandom number generators produced amplitudes and phases with uniform distribution in the ranges

TABLE I. Effects of amplitude and phase jitter on coherences.

Case No.	Case type	$\gamma_T^2(f)$	$\gamma^2(f)$	$\beta^2(f_1, f_2)$
I	Fully coupled	0.999	0.999	0.999
II	Amplitude jitter	0.715	0.460	0.389
III	Phase jitter	0.386	0.322	0.285

$[0,1]$  and  $[0,2\pi]$ , respectively. At least 200 records of 1024 samples were averaged with a 2 Hz frequency resolution.

We consider three cases: full coupling, amplitude jitter, and phase jitter. For full coupling (see case I, Table I), we eliminate jitter by holding phase differences ( $\phi_{fk} - \phi_{dk}$  and  $\phi_{ek} - \phi_{ak} - \phi_{bk}$ ) and amplitude ratios constant ( $d_k/f_k$  and  $a_k b_k/e_k$ ) for each realization. As expected,  $\gamma_T^2(f) \approx 1$ , indicating strong coupling and hence nearly complete predictability of  $v(t)$ . To investigate amplitude jitter (case II, Table I), we hold the phase differences constant, while the ampli-

tude ratios have independent, random variations on the interval  $[0,1]$ . The drop in  $\gamma_T^2(f)$  indicates a loss of coupling. For phase jitter (case III, Table I), we hold amplitude ratios constant, and  $\theta_k$ , hence, the phase differences  $\phi_k = s\theta_k$ , are allowed random variations in the range  $[0,2\pi]$ , where  $s=0.6$ . (As in Sec II D,  $s=1$  yields 0 for all coherences.) The low  $\gamma_T^2(f)$  indicates coupling decay, hence, poor predictability of  $v(t)$ . For high  $\gamma_T^2(f)$ , notice that both  $\gamma^2(f)$  and  $\beta^2(f_1, f_2)$  are high, while low  $\gamma_T^2(f)$  is associated with low  $\gamma^2(f)$  and  $\beta^2(f_1, f_2)$ .

- 
- [1] M. C. Cross and P. C. Hohenberg, *Rev. Mod. Phys.* **65**, 851 (1993).
- [2] J. P. Gollub and R. Ramshankar, in *New Perspectives in Turbulence*, edited by L. Sirovich (Springer-Verlag, New York, 1991), p. 165.
- [3] G. Mayer-Kress and T. Kurz, *Complex Syst.* **1**, 821 (1987).
- [4] S. Narayanan and F. Hussain, *J. Fluid Mech.* **320**, 71 (1996).
- [5] Ch. P. Ritz and E. J. Powers, *Physica D* **20**, 320 (1986).
- [6] R. W. Miksad, F. L. Jones, and E. J. Powers, *Phys. Fluids* **26**, 402 (1983).
- [7] M. Bonetti and J-P. Boon, *Phys. Rev. A* **40**, 3322 (1989).
- [8] J. S. Bendat and A. G. Piersol, *Random Data Analysis and Measurement Procedures*, 2nd ed. (Wiley-Interscience, New York, 1986).
- [9] H. S. Husain and F. Hussain, *J. Fluid Mech.* **304**, 343 (1995).
- [10] K. I. Kim and E. J. Powers, *IEEE Trans. Acoust. Speech Signal Process.* **36**(11), 1758 (1988).
- [11] G. Broze and F. Hussain, *J. Fluid Mech.* **263**, 93 (1994).
- [12] G. Broze and F. Hussain, *J. Fluid Mech.* **311**, 37 (1996).
- [13] A. K. M. F. Hussain, H. S. Husain, K. B. M. Q. Zaman, J. Tso, M. Hayakawa, R. Takaki, and M. A. Z. Hasan, AIAA Paper 86-0235, 1986 (unpublished).
- [14] G. Ahlers, D. S. Cannell, and V. Steinberg, *Phys. Rev. Lett.* **54**, 1373 (1985).
- [15] J. Liu, J. D. Paul, E. Banilower, and J. P. Gollub, in *Proceedings of the First Experimental Chaos Conference*, edited by S. Vohra, M. Spano, M. Schlesinger, L. M. Pecora, and W. Ditto (World Scientific, Singapore, 1992), p. 225.
- [16] J. C. Lasheras and H. Choi, *J. Fluid Mech.* **189**, 53 (1988).
- [17] This was suggested by E. J. Powers in a private communication.